Article

Comparative Study of the Mechanical and Fracturing Behaviors of Shale from Different Gas Blocks in the Longmaxi Formation

Fakai Dou, Peng Hou,* Yanping Wang, Hongbo Zhao, and Chunguang Wang

Read Online

ACCESS | Metrics & More | Article Recommendations

ABSTRACT: With the development of shale gas exploration and exploitation, the mechanical and failure characteristics of shale have become one of the focuses. However, few studies have considered the differences in the mechanical properties of shales in different shale gas blocks. In this study, the effects of bedding orientation on the stress−strain curves, elastic modulus, Poisson's ratio, and fracture morphology of shale samples from the Zhaotong block are analyzed by laboratory experiments, first. Then, a standard deviation method is used to characterize the anisotropy degree of the mechanical and fracturing characteristics of shale. The anisotropy ratio of shale samples between the Zhaotong and Chongqing areas has been comparatively studied. Comparison results show that the shale anisotropy induced by the bedding orientations demonstrates apparent regional characteristics. There are significant differences in the mechanical properties of shale obtained from different shale gas blocks. It indicates that the optimization of engineering practices such as the design of hydraulic fracturing should consider the influences of the bedding orientations and shale gas blocks on the shale anisotropy.
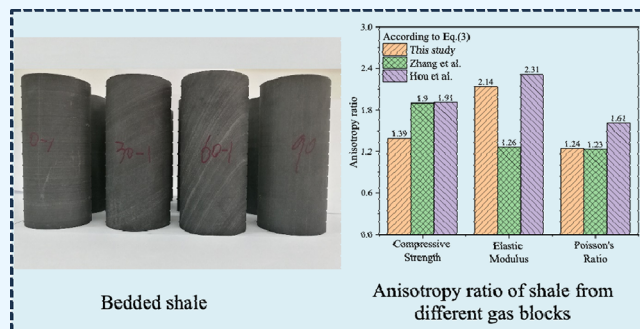
1. INTRODUCTION

Shale gas is one of the alternatives to conventional natural gas. The successful exploitation of shale gas from deep reservoirs has attracted an increasing amount of attention around the world. Due to the difference in sedimentary minerals, climate change, and the stress field, the mineral composition inside the shale formation behaves relatively complex and variable. Some shale formation contains rich organic matter, it may be gray or black. Comparatively, if the shale contains rich iron, it may show brown-red. The mineral composition within the shale matrix affects not only the apparent characteristics of the rock but also the mechanical characteristics.[1] Due to the geological evolution processes, the parallel arrangement of clay minerals generates laminated structures in the shale formation. The different physical properties and mechanical parameters in different directions make the shale anisotropy much more distinct.[2,3] Therefore, the understanding of the shale mechanical and fracturing behaviors becomes more and more essential for the recovery of hydrocarbons from deep reservoirs.

Experimental research on shale physical properties and mechanical parameters is mainly completed by using field-emission scanning electron microscopy (FE-SEM), X-ray diffraction tests, and conventional mechanical tests. It has been proved that the shales are mainly composed of quartz, carbonate, clay, and organic matter.[4,5] The shale anisotropy induced by the mineral compositions ranges from pore level to reservoir level, which enhances the difficulty in quantifying shale anisotropy degree.[6−8] The contents of clay and organic matter not only directly affect the rock strength but also have a positive relationship with the porosity that exerts important influences on permeability.[9] In addition, the shale samples with abundant quartz or carbonate show more obvious brittle characteristics than those samples with abundant clay.[10,11] It indicates that the micromechanical properties of brittle minerals could directly affect the macro brittle characteristics of shale samples. By investigating shale samples adopted from different areas in North America, Sone and Zoback[12,13] found that the elastic properties tend to be more anisotropic if the shale samples contain high contents of clay and organic matter. Based on the uniaxial and triaxial compression tests, Alsuwaidi et al.[14] experimentally studied the mechanical behaviors of shale samples from the Laffan and the Nahr Umr areas and concluded that the shale strength and elastic anisotropy obey a function of bedding orientations. They also emphasized that the transverse isotropy assumption is suitable to describe the shale samples.

The fracturing behaviors of shale samples are mainly affected by the orientation of laminated structures.[15] With the help of acoustic emission (AE) technologies, the researchers could easily study the fracturing behaviors of rock samples under different loading circumstances. Kaiser and Kim[16] found that brittle failure processes tend to get suppressed when the stress ratio (σ_1/σ_3) decreases to a threshold or the confining pressure beyond UCS/10. Under these circumstances, the final failure morphology of rock samples is associated with a macroscopic shear failure. Amann et al.[17] investigated the mechanical behaviors of clay shale under the uniaxial compression tests and found that the crack initiation and damage thresholds of clay shale in the Mont Terri Underground Research Laboratory are 30 and 70%, respectively. Additionally, the crack initiation is mainly affected by the differential stress rather than the confining pressure under the triaxial compression tests.[18] Except for the mineral components, some other factors also affect the shale fracturing characteristics such as the water content. By using the AE technology, Chen et al.[19] found that the failure mode of shale samples is much more easily transiting from tension failure to tension-shear mixed failure if the water content of shale samples is a little high. The stress path also affects the crack propagation process in the construction of the deep gas reservoirs. Duan et al.[20] experimentally studied the effects of loading cycles on the energy evolutions of anisotropic phyllite samples under triaxial compression tests. They found that the elastic strain energy and the dissipated strain energy increase with increasing cyclic number, which reflects the crack generation and propagation of microcracks. The loading conditions also affect the rock permeability. The rock permeability may vary more than 2 orders of magnitude under different stress paths.[21,22]

Since 2010, Chinese researchers have started the shale gas exploration and found that there are several huge shale gas reservoirs (Sichuan and Chongqing in the southwest, Xinjiang in the northwest, and the Songliao Basin in the northeast) buried in the mainland of China.[23-25] Due to the differences in the depositional history of shale formations, shale formation exhibits distinct heterogeneity and anisotropy. The insufficient geomechanical investigations disturb the process of shale gas exploration and exploitation, to some extent. Up to now, the number of commercially developed shale gas blocks has still few. These developed shale gas blocks are mainly distributed in Fuling, Changning, Weiyuan, Fushun-Yongchuan, and Zhaotong.[26,27] The previous research highlights mainly focus on the Longmaxi shale formation, especially in the Chongqing area because of the early exploration.

Many researchers have investigated shale's mechanical properties based on conventional compression tests. However, the shale anisotropy is exhibited not only at the sample scale but also at the formation scale. Owing to the rapid exploitation of shale gas/oil, investigations of the shale anisotropy degree remain lagging in guiding the hydraulic fracturing operations. As we know, the shale mechanical properties could directly affect the failure strength in the reservoir fracturing activities and the complexity of the fracture network after loading, which could affect the migration pathways of shale gas and the production efficiency of reservoirs. To decrease the substantial errors in engineering applications, the shale anisotropy degree of the mechanical properties at the formation scale should be considered before the start of exploitation. This study mainly focuses on the comparison of shale mechanical properties among different shale gas blocks and uses a new method to analyze the difference in their anisotropy degree quantitatively. The effects of bedding orientations on the mechanical properties and fracturing behavior of shale samples from the Zhaotong block are studied by laboratory experiments, first. Then, by comparing the shale mechanical properties obtained from the Zhaotong and Chongqing areas, the differences in shale anisotropy degree at the formation scale are deeply discussed in this study, which could improve the reservoir stimulation efficiency much more obviously.

2. PREPARATION OF EXPERIMENTAL TESTS

2.1. Sample Preparation and Characterization. The conventional triaxial compression tests aim to investigate the influence of the dip angle of the shale bedding plane on its compressive strength, elastic modulus, Poisson's ratio, and failure mode. Therefore, the shale samples should be prepared according to the ASTM. First, the shale rock should be processed into a cylindrical sample with a diameter of 50 mm and a height of 100 mm. Then, the upper and lower ends of the shale sample should be processed as parallel, the diameter error along the height direction of the shale sample should be smaller than 0.3 mm, the end face should be perpendicular to the axis of the sample, and the deviation should be smaller than 0.25°. Finally, only those samples with intact and smooth surfaces could be accepted. This study defines the angle between the bedding plane and the horizontal plane as the dip angle. Based on previous experimental studies,[28-31] four typical dip angles of the shale samples are selected, that is, 0°, 30°, 60°, and 90°. Figure 1 shows the front and top views of shale samples after
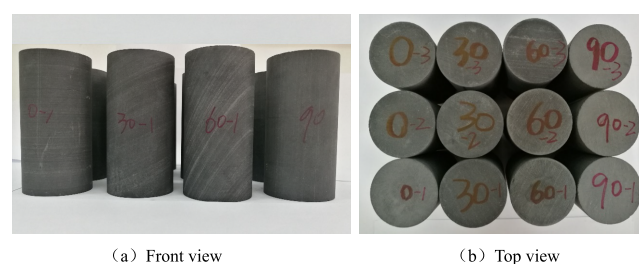

Figure 1. Shale samples have different bedding orientations. (a) Front view. (b) Top view.

cutting and grinding. As shown in Figure 1, the surfaces of these samples are intact and smooth, and the layered structures are visible.

The physical parameters of shale samples such as their diameter, height, mass, and P-wave velocity should be measured before the loading procedure. As shown in Figure 2a,b, the differences in diameter and height among each sample are within 0.5 and 1 mm, respectively. The loading rate is decided by the loading strain rate; therefore, the size differences of sample heights have no effects on experimental results. The density of these shale samples is 2.65 g/cm^3 by measuring the mass (in Figure 2c) and the sizes of the shale samples.

Previous investigations have proved that the natural fractures and bedding could reduce the velocity of ultrasonic waves.[32,33] Here, the P-wave speed is used to measure the internal integrity of the shale sample before the compression test, which eliminates samples with internal invisible cracks and guarantees the reliability of the experimental results before compression. The value of P-wave speed is affected by the orientation of bedding and internal microfractures. If there are many internal
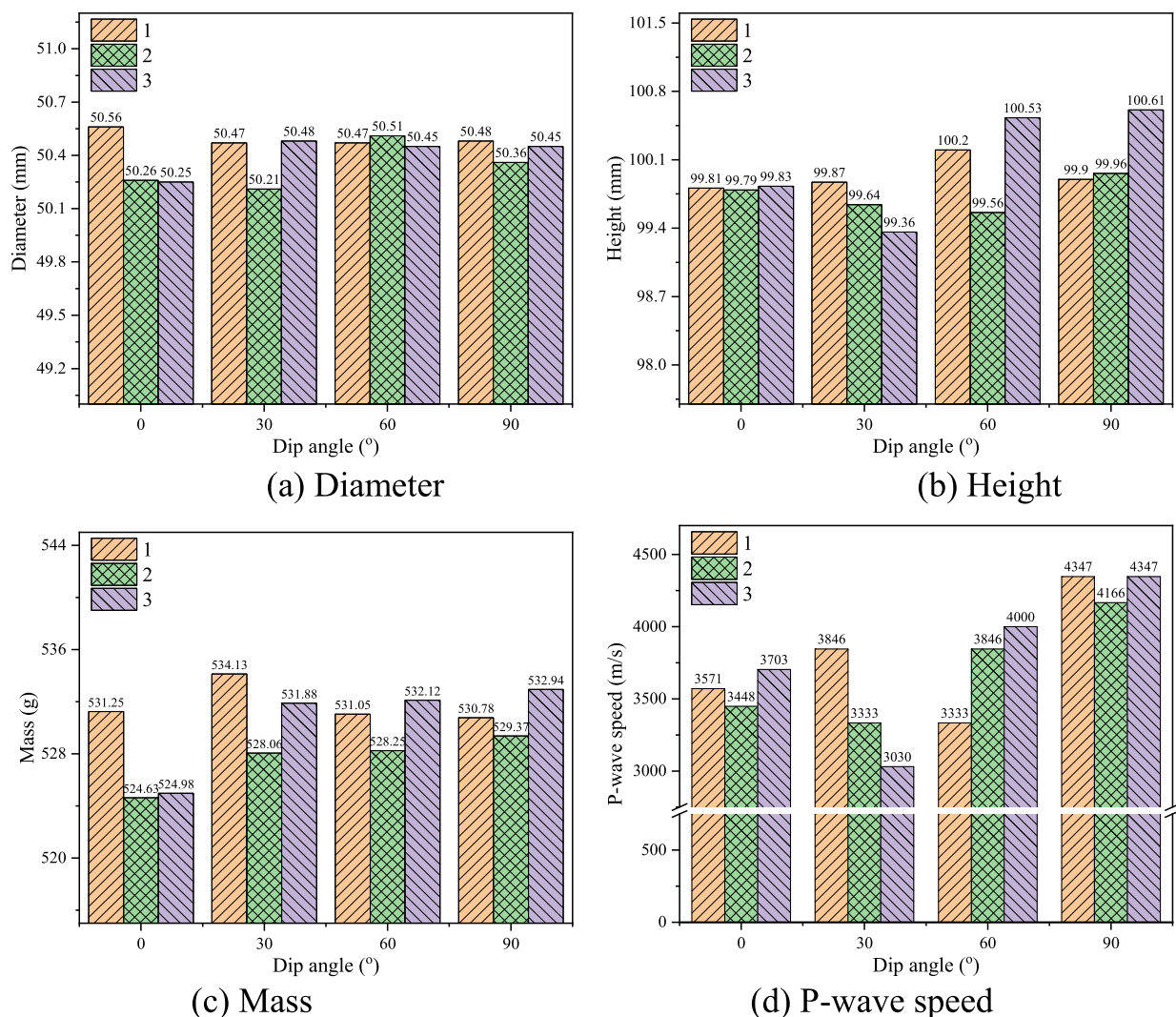
(a) Diameter

(b) Height

(c) Mass

(d) P-wave speed

Figure 2. Physical parameters of shale samples. (a) Diameter. (b) Height. (c) Mass. (d) P-wave speed.
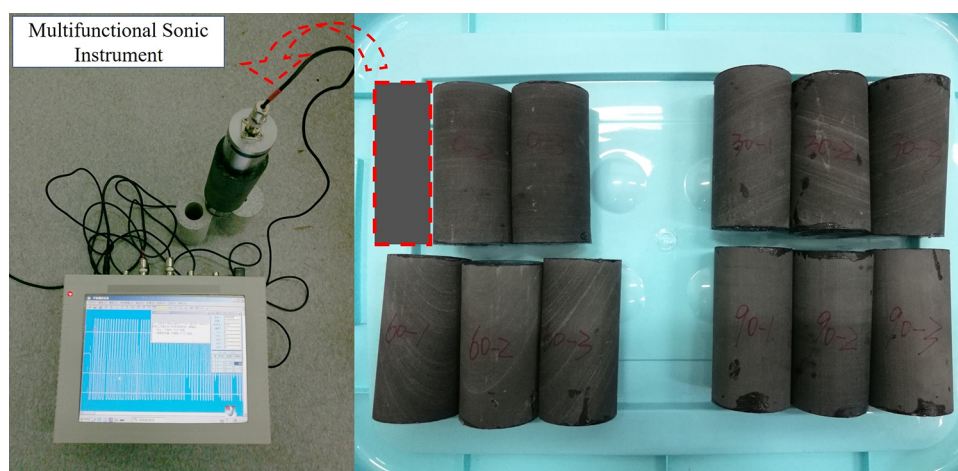

Figure 3. Measurement of the shale sample for P-wave speed.

fractures distributed in the internal shale samples, the P-wave speed will be dropped obviously. If the beddings are parallel to the direction of wave propagation, then the P-wave speed is relatively high. Figure 2d shows the P-wave speed of each shale sample, which is measured by a multifunctional sonic instrument in Figure 3. Those shale samples with obvious natural defects will be excluded before starting the loading test.

2.2. Experimental Set Up and Procedure. These conventional triaxial compression tests were completed by the electro-hydraulic servo-controlled rock mechanics testing
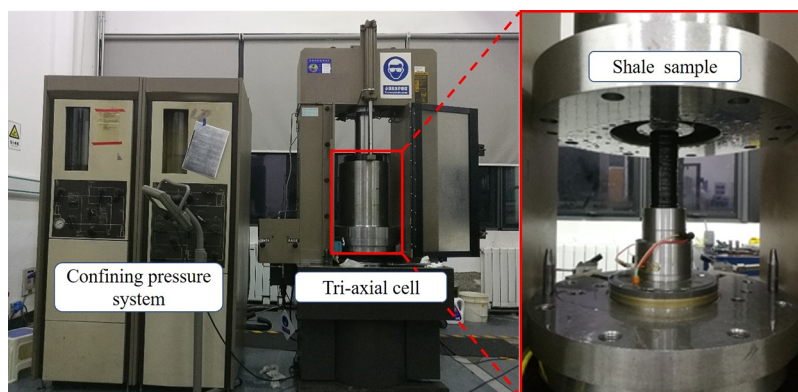
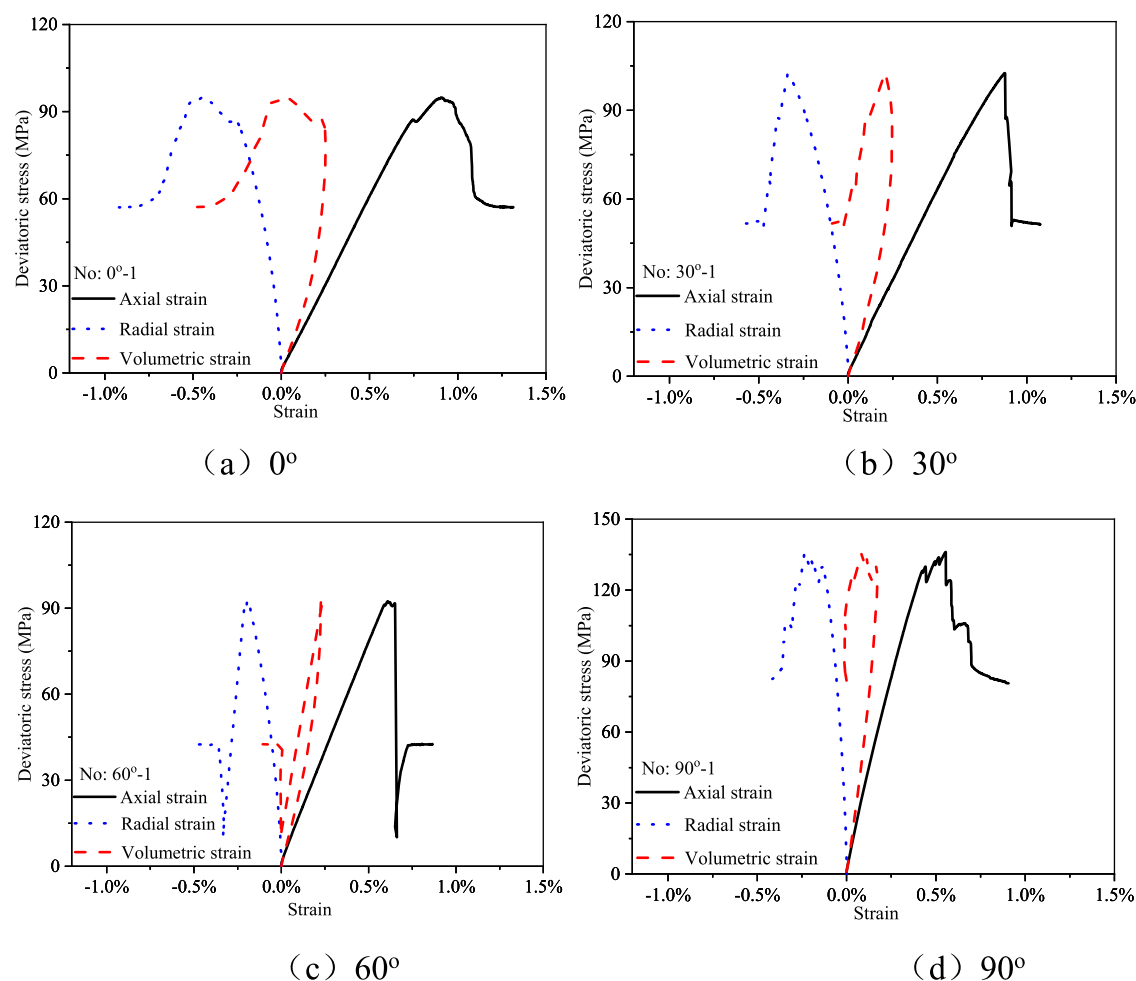**Figure 4.** Electro-hydraulic servo-controlled testing system for rock mechanics.

Figure 5. Stress−strain curves of shale samples under different dip angles. (a) 0°. (b) 30°. (c) 60°. (d) 90°.

system (MTS 815) and its real photo is shown in Figure 4. The test system is composed of a host computer, multichannel controller, pressure control cabinet, and hydraulic oil source, which can apply a maximum axial force of 1700 kN and a maximum confining pressure of 45 MPa. The stiffness of the mainframe of the test system is 10.5×10^9 N/m, the power of the hydraulic source is 18 kW, and the flow rate of the hydraulic source is 31.8 L/min.

Before the loading process, the shale samples should be protected by oil proof. Usually, the shale samples will be wrapped by two layers of thermoplastic film, and the electrical insulating tape is in the middle. After the oil-proof process, the protected shale sample should be located in the test platform, and the hoop strain gauge should surround the center of the sample. In addition, the corresponding information on the shale sample also needs input from the main control computer. During the quasi-static loading process, the confining pressure is set to 20 MPa under a loading rate of 0.05 MPa/s and the loading plate moves along the geometric axis of the shale sample under a loading strain rate of 0.0007% each second.

3. MECHANICAL AND FRACTURING BEHAVIORS OF SHALE

3.1. Mechanical Properties. The stress−strain relationship is the basic information for studying rock strength and deformation characteristics. According to conventional triaxial compression tests, the stress−strain relationship curves of shale samples under four different dip angles of the bedding plane were obtained. Figure 5 shows the stress−strain curves of shale samples from the aspect of axial strain, radial strain, and volumetric strain, which are described by the black solid line, blue dotted line, and red dashed line. Take the axial strain as an example, these stress−strain curves show an obvious linear growth stage in the early stage of the loading process. With the increase of axial stress, these curves of shale samples begin to change, especially when the axial stress approaches the peak stress. As shown in Figure 5a, the axial stress presents nonlinear characteristics at the stage close to the peak stress when the dip angle is 0°. Here, the peak stress is regarded as the compressive strength of shale under conventional compression tests. The axial strain shows a sudden increase, and the axial stress shows a slowly decreasing trend at the beginning of the postpeak stage. When the residual strength decreases to 62 MPa, the axial strain approaches 1.1%. It indicates that the shale sample shows plastic failure characteristics to some extent when the loading direction is vertical to the bedding planes. When the dip angle is 30°, the linear growth characteristic of the axial stress before the peak stress in Figure 5b is more obvious than that in Figure 5a, and the axial stress shows a precipitous descent after the peak stress. Under this circumstance, the shale sample shows brittle failure characteristics and its residual strength drops to 52 MPa with 0.92% axial strain.

When the dip angle of the bedding plane is 60° (seen in Figure 5c), the brittle failure characteristics of the shale become much more obvious. Whether the axial stress approaches the peak stress or after the peak stress, the relationship between stress and strain is almost linear. The residual strength decreased abruptly to 10 MPa, which reflects the suddenness of rock failure. Then, the residual strength rebounded quickly to 42 MPa and remained stable due to the confining pressure. At the moment of rock destruction, the axial strain of the shale sample was 0.73%. When the dip angle of the bedding plane is 90° (seen in Figure 5d), the stress−strain curve shows many small fluctuations in the process of gradually approaching the peak stress. Even in the postpeak stage, the stress−strain relationship of shale still fluctuates visibly. It indicates that the crack propagation process did not complete instantaneously. The above curves indicate that the influences of bedding orientation on the stress−strain relationship are mainly reflected in the destruction stage, especially the postpeak stage. The fluctuation of the stress−strain curve after peak strength is the reflection of the fracturing behaviors of shale samples.

Figure 6 concludes the effects of the bedding orientations (0°, 30°, 60°, 90°) on the shale compressive strength under the confining pressure of 20 MPa. For each dip angle of beddings, there are three experimental results of shale samples involved in the comparison. As shown in Figure 6, the three experimental results are represented by squares, circles, and triangles, while the bold circle is their average value. The average values of compressive strength under different dip angles are connected by the dashed line, which can better reflect the variation trend of shale compressive strength under different dip angles of the bedding plane. The experimental results of shale compressive
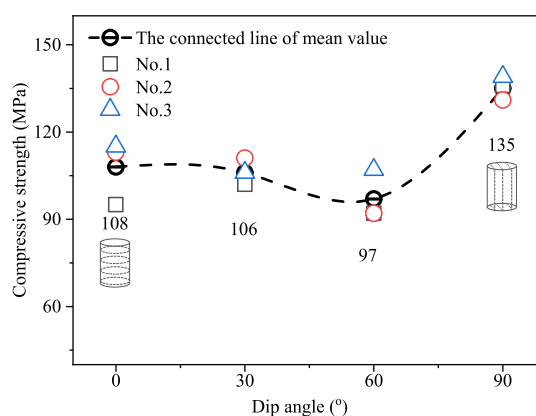

Figure 6. Bedding orientation's effects on shale samples' compressive strength.

strength did not show an obvious "U-shaped" variation trend. It can be seen from the test results that the compressive strength of shale in the conventional triaxial compression test first decreases slowly and then increases obviously as the dip angle increases from 0° to 90°. When the dip angle of the bedding plane is 60°, the compressive strength of the shale is the lowest, and the dispersion of the test results is the largest. Under this circumstance, the shale compressive strength fluctuates from 92 to 107 MPa, which is directly affected by the strength difference of bedding planes. When the loading direction is parallel to the bedding planes (the dip angle is 90°), the average value of the shale compressive strength is 135 MPa, which is the highest compressive strength of any other dip angle.

The orientation of beddings not only affects the failure process and the compressive strength of shale samples but also the elastic modulus and Poisson's ratio. Figure 7 reflects the
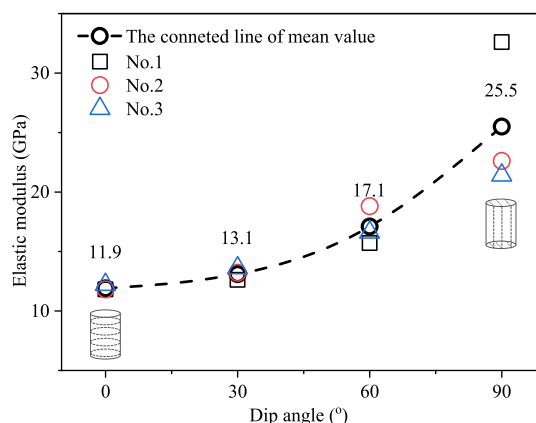

Figure 7. Effects of the bedding orientation on the elastic modulus of shale samples.

influence of the dip angle of the bedding plane on the shale elastic modulus. When the dip angle of the bedding plane increases from 0° to 90°, the elastic modulus of shale samples and its growth rate increase gradually according to the experimental results of conventional compressive tests. When the dip angle of the bedding plane is 0°, the experimental results vary little, and the average elastic modulus of the shale sample is 11.9 GPa, which is the lowest of any other circumstances. With the increase of the dip angle, the dispersion of test results also starts to increase. When the dip angle is 90°, the average elastic modulus of the shale sample is 25.5 GPa, which is the largest of

any other circumstances. Additionally, the test results vary greatly under the same loading conditions. Affected by the relationship between the bedding orientation and the loading direction, the maximum elastic modulus of the shale sample is about 114% higher than the minimum elastic modulus under the same confining pressure. It indicates that the shale sample shows obvious anisotropic characteristics.

Figure 8 reflects the influence of the bedding orientation on Poisson's ratio of shale. Under the same loading conditions,
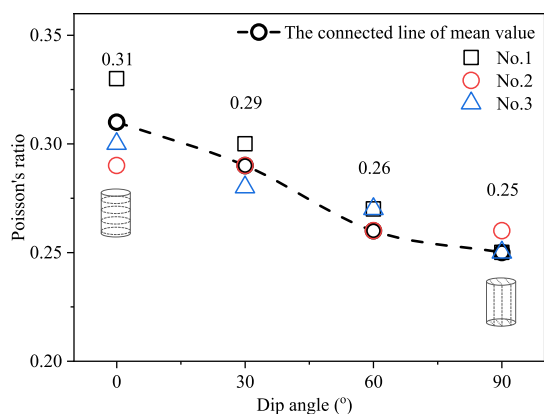

Figure 8. Effects of the bedding orientation on Poisson's ratio of shale samples.

Poisson's ratio of shale samples decreases linearly from 0.31 to 0.25 as the dip angle of the bedding plane increases from 0° to 90°. Compared with the variation trend of elastic modulus in Figure 7, the variation trend of Poisson's ratio under different dip angles is opposite to the elastic modulus in Figure 8.

3.2. Fracture Morphology. The bedding orientation's effects on the fracture morphology are compared in this chapter. Under the same conventional triaxial compression tests, the macroscopic fracture morphologies of all of the shale samples are compared in Figure 9.

Take Figure 9a as an example; it shows the final fracture morphologies of three shale samples from the front and backside. When the dip angle of the bedding plane is 0°, the propagation paths of the main fractures are not smooth. As shown in Figure 9a-1, two main fractures start 3 cm from the top side of the shale sample. One of the main fractures penetrates the shale sample from the middle while the other main fracture penetrates the shale sample from the bottom. The angle between the end of the main fractures and the horizontal is approximately 50°. The main fractures in Figure 9a-2 have two branches that appear at the two ends of the main fracture. The propagation paths of these branches are also torturous. Figure 9a-3 shows the front and back sides of the third shale sample, which exhibits a main penetrating fracture and lots of tortuous fracture branches. Overall, the uneven propagation path of the fractures means that the brittle failure characteristics of the shale sample are not obvious when the dip angle of the bedding plane is 0°.

When the dip angle of the bedding plane is 30° (Figure 9b), the morphologies of the main fracture surface are simple. After loading, the fractures in the shale samples are mainly smooth, penetrating fractures rather than fracture branches. Under this circumstance, the angle between the end of the main fractures and the horizontal is approximately 70°.

When the dip angle of the bedding plane is 60° (Figure 9c), the shale sample shears directly along the bedding plane. There
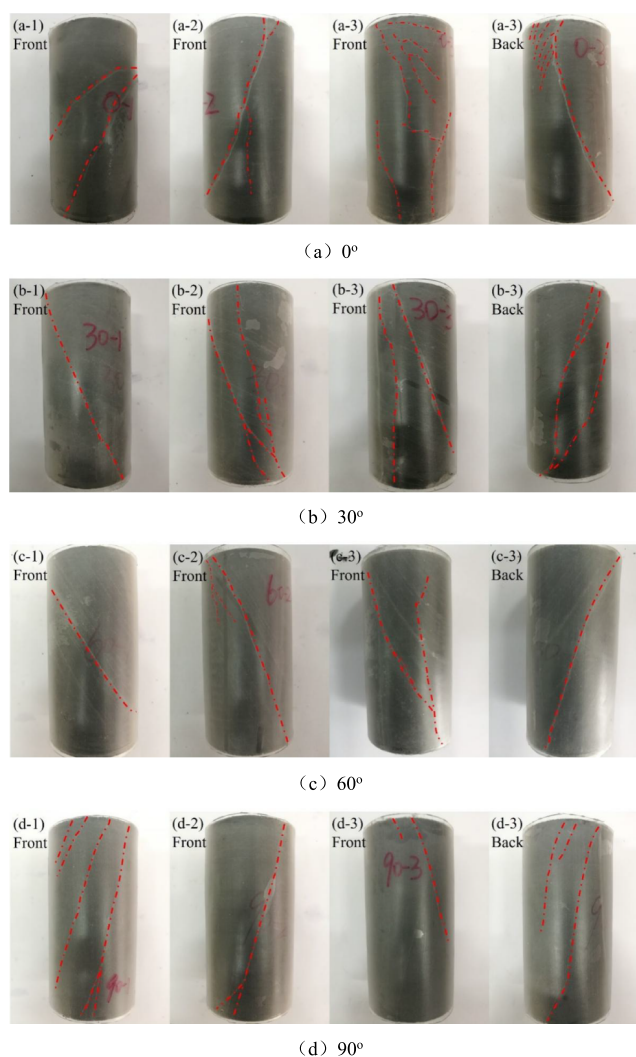

Figure 9. Fracture morphologies of shale samples under different bedding orientations. (a) 0°. (b) 30°. (c) 60°. (d) 90°.

will be a few cracks parallel to the bedding plane or loading direction. Additionally, the number of fractures under this dip angle is the least and the smoothest.

When the dip angle of the bedding plane is 90° (Figure 9d), the main fractures are initiated from the top side and penetrate the shale sample to the bottom side. The fracture branches are relatively simple and straight, which is parallel to the main fracture. In addition, the propagation direction of these fractures is more likely to approach the loading direction.

3.3. Fractal Dimension. To accurately compare the differences in the final fracture morphology of shale samples under conventional triaxial compression tests, the complexity of the final fracture morphology of these shale samples is quantified by the fractal dimension. There are many definitions of the fractal dimension. Here, we used the Hausdorff fractal dimension by using the box-counting method.

The characteristics of fracture sizes and tortuous degrees have already been described by the solid line in Figure 10. The thickness of solid lines in the binary images is used to reflect the damage degree caused by the fractures. That is to say the thick lines represent main cracks and thin lines represent branch cracks. These three-dimensional fracture networks were projected into two-dimensional fracture images. First, the fracture morphologies should be extracted separately in the
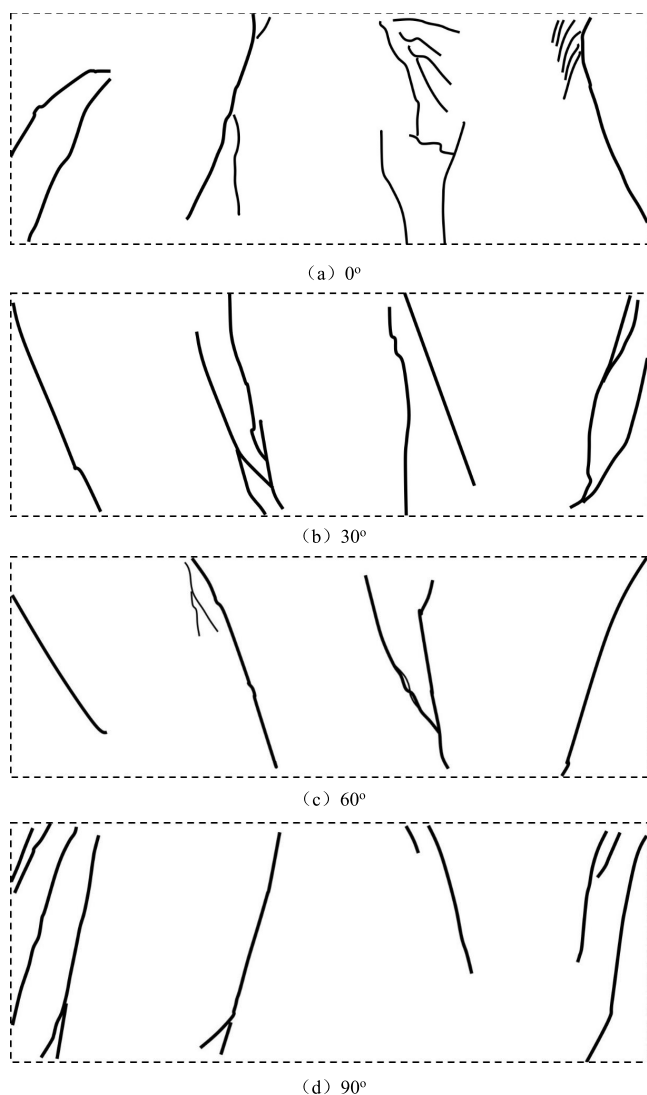
Figure 10. Binary images of the fracture morphologies under different bedding orientations. (a) 0°. (b) 30°. (c) 60°. (d) 90°.

white background of the binary image. Then, the binary image should be pretreated. Finally, the reversed binary image should be imported into the Fraclab toolbox in MATLAB. It means that the nonzero pixels belong to the object (fractures) and the zero pixels constitute the background.

The algorithm of the box-counting method could be concluded in eq 1 and the detailed steps in the Fraclab toolbox are as follows[34]:

$$D = \lim_{n \to \infty} \frac{\lg M(n)}{n \lg 2} \qquad (1)$$

(1) Pad the reversal binary image by 2^n boxes and the size of the box is $1/2^n$. Here, in this study, the value of n is 9, which means that each binary image is divided into lots of pixel boxes ranging from 2 to 512.

(2) Compute the $M(n)$, which represents the number of boxes of size $1/2^n$ that contain at least one nonzero pixel.

(3) Reduce the size of the box to $1/2$ its original size and repeat step 2.

(4) Compute the points of $\log M(n)$ and $\log 2^n$ use the least-squares method to fit a line to the points.

(5) The Hausdorff fractal dimension D is the slope of the line in step 4.

Figure 11 concludes that the effects of the dip angle on the fractal dimension of the final fracture morphology of shale
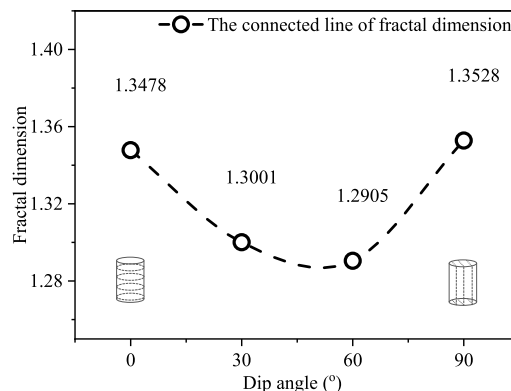

Figure 11. Fractal dimension of shale samples under different bedding orientations.

samples. As the dip angle increases from 0° to 90°, the fractal dimension of the final fracture morphology decreases first and then increases. Generally, the variation of fractal dimension shows a "U-shaped" trend. It indicates that no matter the loading direction parallel or vertical to the shale sample, the complexity of final fracture morphologies is about 1.35, which is relatively high. When the dip angle of beddings ranges from 30° to 60°, the fractal dimension of these final fractures is around 1.30, which indicates the fracture morphologies are relatively simple and the brittle failure features are obvious.

4. RESULTS DISCUSSION

Some researchers have carried out the same conventional triaxial compression tests as in this study to investigate the shale anisotropy characteristics. To explore the differences in the anisotropy of shale in different shale gas blocks, the experimental results of Zhang et al.[30] and Hou[31] are compared with our experimental results. Their samples are obtained from the Chongqing area. The size of the shale samples and the loading conditions are consistent with this study adopted from the Zhaotong area. Under these circumstances, the comparison of the effects of dip angle on the compressive strength, elastic modulus, and Poisson's ratio of the shale samples are discussed in the following.

4.1. Compressive Strength. This section compares the variation of shale compressive strength as the dip angle increases from 0° to 90°. Three different triaxial compression test results are given in Figure 12. To some extent, the variation trend of the strength curve in this study is similar to the results of Hou,[31] represented by the red dotted line. For these two results, the shale compressive strength decreases first and then increases. The inflection points of these two curves occur around 60° and show a "U-shaped" variation trend. However, these two curves' strength values and related ranges differ significantly. Under the same loading conditions, the shale compressive strength in the Zhaotong area increases from 97 to 135 MPa, and the range is 38 MPa. While the shale compressive strength in the study of Hou[31] increases from 111 to 212 MPa, and the range is 101 MPa. Comparatively, Zhang[30] also focused on the shale strength in the Chongqing area. However, the shale compressive strength shows a "W-shaped" variation trend as the dip angle increases
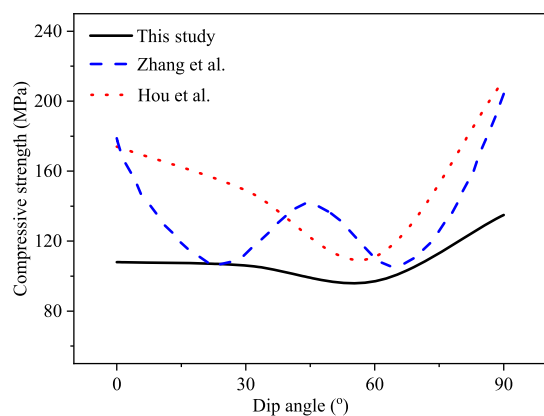
Figure 12. Comparison of the shale compressive strength under different dip angles.

from 0° to 90°. In addition, the magnitude of the shale compressive strength fluctuates considerably. The shale compressive strength in the blue dashed line increases from 106 to 204 MPa, and the range is 98 MPa. Although the red dotted line and blue dashed line reflect the shale compressive strength in the Chongqing area, respectively, the variation trend shows a significant difference. It indicates that the shale strength anisotropy induced by beddings is apparent and regional.

4.2. Elastic Modulus. This section investigates the elastic modulus of shale with different bedding orientations. In Figure 13, the shale elastic modulus in various studies increases with the
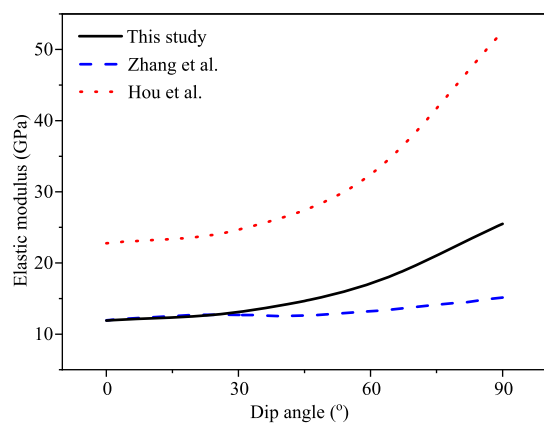

Figure 13. Comparison of shale elastic modulus under different dip angles.

increase of dip angles and the slope of the growth curve varies significantly. For example, when the dip angle is 0° or 30°, the differences in the elastic modulus between the solid black line and the dashed blue line are negligible. However, as the dip angle increases from 0° to 90°, the elastic modulus of shale in the Zhaotong area (solid black line) increases from 12 to 26 GPa, which increases by 116.7%. In comparison, the elastic modulus of shale in the Chongqing area (dashed blue line) increases from 11 to 15 GPa, which increases by 36.4%. The dotted red line in Figure 13 also reflects the variation of the shale elastic modulus from the Chongqing area. Under this circumstance, the average value is high, and the growth rate of the shale elastic modulus is high. The shale elastic modulus increased from 23 to 53 GPa, which increases by 130.4%. By comparing the variation trend of shale elastic modulus in three studies, the elastic modulus of shale from different regions could be similar at certain dip angles.

The differences mainly occur at high dip angles. In addition, the shale elastic modulus changes little as the dip angle ranges from 0° to 30°.

4.3. Poisson's Ratio. This section compares the shale Poisson's ratio with different bedding orientations. In Figure 14,
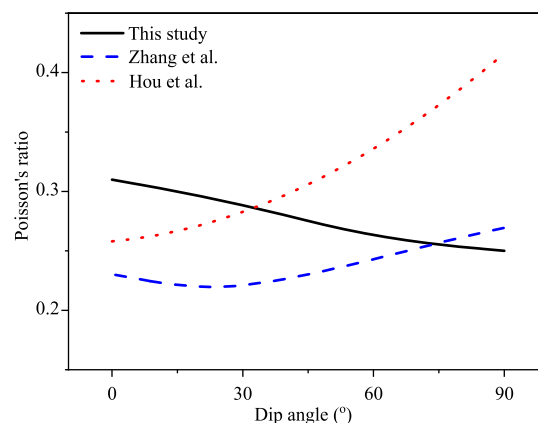

Figure 14. Comparison of shale Poisson's ratio under different dip angles.

with the increase of dip angle, the variation trends of shale Poisson's ratio in these three tests are quite different. For the black dashed line, the shale Poisson's ratio decreases linearly from 0.31 to 0.25 as the dip angle increases from 0° to 90°, which decreases by 19.4%. For the dashed blue line, the shale Poisson's ratio decreases from 0.23 to 0.22 and then increases to 0.27. The stagnation point of the curve approaches 30°. For the dotted red line, the shale Poisson's ratio grows monotonically from 0.26 to 0.42, and the growth rate becomes more significant as the dip angle increases. Under this circumstance, the shale Poisson's ratio increase is about 61.5%. The anisotropy of Poisson's ratio may closely relate to the distribution, orientation, and closure state of microcracks inside the rock. The shale Poisson's ratio demonstrates prominent anisotropy characteristics by comparing the variation trend of curves in three studies. It indicates that even under the same confining pressures the shale deformation and destruction may show a noticeable difference because of the irregular distribution of pores or cracks at the microscale level.

4.4. Anisotropy Ratio. Most researchers define the anisotropy ratio (AR) as the ratio between the rock properties measured vertically to the stratified structures and those measured parallel to the stratified structure.[35] For example, some researchers prefer to define the strength AR as the ratio of the obtained shale compressive strength between 90° and 0° as expressed in eq 2. In contrast, some other researchers prefer to adopt the AR defined as the ratio of the obtained index of mechanical properties between the maximum value and the minimum value, as expressed in eq 3:

$$AR = \frac{\sigma_{90}}{\sigma_0} \tag{2}$$

$$AR = \frac{\sigma_{max}}{\sigma_{min}} \tag{3}$$

According to the previous definition of the AR, the more significant the difference between the AR and 1, the more pronounced the rock anisotropy is. This index is good at reflecting the monotonically changing trend of rock properties with bedding orientations. However, some test results indicated
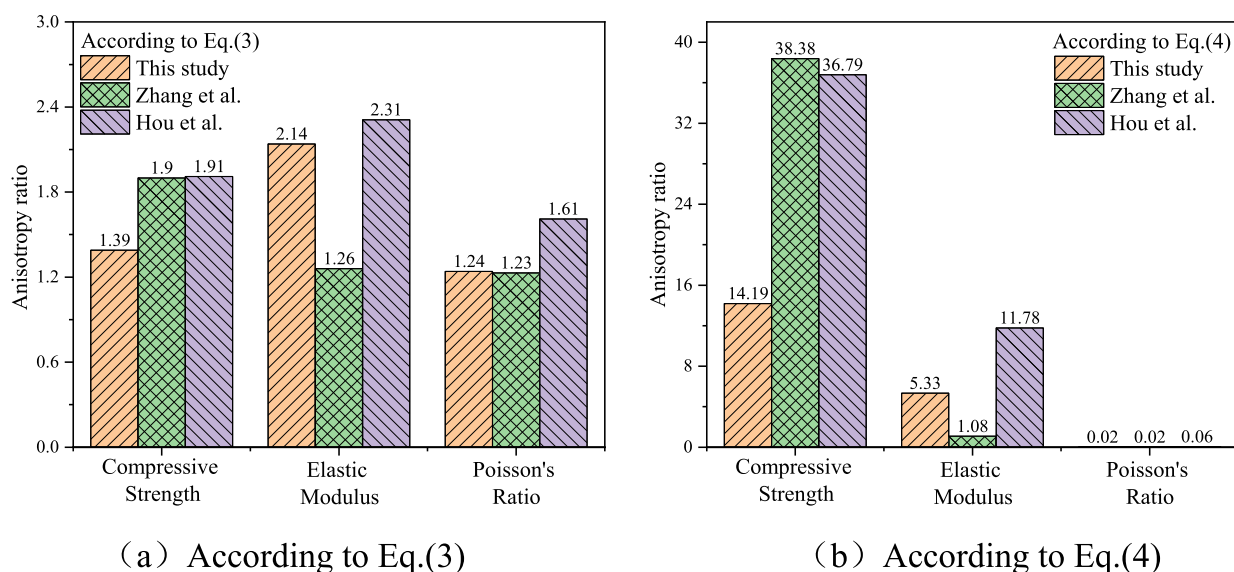
（a）According to Eq.(3)   （b）According to Eq.(4)

Figure 15. Comparison of anisotropy ratios under different equations. (a) According to eq 3. (b) According to eq 4.

that the shale properties might show a "U-shaped" or "W-shaped" variation trend as the dip angles increase. For these circumstances, the previous definitions of the AR hardly reflect the effects of dip angles on the anisotropy characteristics. Therefore, this study adopts a standard deviation method to better reflect the anisotropic shale properties, which could better reflect the nonmonotonic trend of shale characteristics under different dip angles:

$$ AR = \sqrt{\frac{\sum_{i=1}^{n}(x_i - \overline{x})^2}{n}} \qquad (4) $$

where x_i means the value of the index of layered rock properties, i means the serial number of different dip angles, n represents the number of different dip angles, and $\overline{x}$ means the average value of the index of layered rock properties. According to eqs 3 and 4, the comparison of the AR of different mechanical properties is shown in Figure 15.

In Figure 15a, the anisotropy degrees of shale mechanical properties in different production areas seem relatively similar. Two kinds of shale samples in different regions may show similar anisotropic degrees for each shale's mechanical property. According to eq 3, the AR of different shale mechanical properties does not tend to change in multiples. However, the anisotropy degree of shale mechanical properties in different production areas obviously varies, as shown in Figure 15b. According to eq 4, the AR of different shale mechanical properties tends to fluctuate in multiples. The reason is that eq 3 emphasizes the difference between the maximum and the minimum values, while eq 4 highlights the difference between the individual measured and their average values. Compared with the variation trend of shale mechanical properties in Figures 12−14, the AR presented in Figure 15b could reflect the shale anisotropic degree induced by bedding orientations in a more intuitive way. That is to say, the proposed anisotropic ratio in this study (refer to eq 4) could better show the influences of the dip angles on the shale anisotropic properties.

Generally, shale bedding anisotropy and reservoir heterogeneity have apparent regional characteristics. Through experimental study and comparative analysis of the conventional triaxial compression test results of shale, the regional differences

in the anisotropy degree of shale are noticeable. Due to the differences in the depositional stages of shale formation, there are many differences in the mineral composition of shale gas reservoirs among different blocks even at different depths of the same block. Therefore, studying the shale fracture propagation process should consider not only the bedding orientations but also the matrix heterogeneity. It helps greatly to understand better the failure mechanism of shale in different formations, which has a positive influence on the optimization of field fracturing design and construction.

5. CONCLUSIONS

This study investigated the differences in the anisotropy degree of the dry shale samples among different shale gas blocks. Based on the experimental results and comparative analysis, conclusions can be drawn as follows:

The influence of bedding orientation on the shape of stress−strain curves occurs in the postpeak stage, which directly impacts the complexity of the shale final fracture morphology. As the dip angle increases from 0° to 90°, the shale compressive strength shows an obvious "J-shaped" variation trend, while the fractal dimension shows a "U-shaped" variation trend. When the dip angle is around 60°, the shale failure is mainly determined by bedding strength rather than matrix. Under this circumstance, the measured values of the shale compressive strength are the lowest and the most discrete. The variation trend of the elastic modulus is similar to a concave function, and the ratio of maximum to minimum elastic modulus is about 2.14. Additionally, Poisson's ratio of shale samples decreases linearly as the dip angle increases.

The complexity of the crack propagation path of these shale samples has been quantified by the fractal dimension. The "U-shaped" variation trend of the fractal dimension proves that the fracture morphology will be more complex if the shale failure mainly occurs in the matrix part rather than bedding planes. If the fracturing behaviors mainly occur in beddings, the fracture morphologies will be simple with little ductile deformation.

The reconstruction of the shale gas reservoir should consider the regional characteristics of the shale anisotropy degree rather than directly copy the shale mechanical properties in the existing literature. The comparative study reveals that the traditional

calculation method of the AR is good at reflecting the differences between the maximum and the minimum values of the rock properties, while the proposed AR could better reflect the individual differences from the average, especially when the number of rock samples is very large.

■ AUTHOR INFORMATION

Corresponding Author

Peng Hou — *School of Civil Engineering, Wuhan University, Wuhan 430072, China;* ⓘ orcid.org/0000-0002-2752-3958; Email: penghou@whu.edu.cn, phou1989@163.com

Authors

Fakai Dou — *School of Civil Engineering and Geomatics, Shandong University of Technology, Zibo 255000, China*
Yanping Wang — *School of Civil Engineering and Geomatics, Shandong University of Technology, Zibo 255000, China*
Hongbo Zhao — *School of Civil Engineering and Geomatics, Shandong University of Technology, Zibo 255000, China*
Chunguang Wang — *School of Civil Engineering and Geomatics, Shandong University of Technology, Zibo 255000, China*

Complete contact information is available at:
https://pubs.acs.org/10.1021/acsomega.3c06867

Author Contributions

F.K.D.: conceptualization, data analysis and processing, writing the original draft. P.H.: conceptualization, investigation, methodology, supervision, writing, reviewing, and editing the manuscript. Y.P.W.: conceptualization and reviewing the manuscript. H.B.Z.: methodology, supervision, and reviewing the manuscript. C.G.W.: investigation and reviewing the manuscript.

Notes

The authors declare no competing financial interest.

■ ABBREVIATIONS

FE-SEM, field-emission scanning electron microscopy; AE, acoustic emission

■ REFERENCES

(1) Dou, F. K.; Hou, P.; Jia, Z. R.; Wang, C. G.; Zhao, H. B.; Wang, Y. P. Effect of clay minerals on tensile failure characteristics of shale. *ACS omega.* **2022**, 7 (28), 24219−24230.

(2) Barton, N.; Quadros, E. Anisotropy is everywhere, to see, to measure, and to model. *Rock Mech Rock Eng.* **2015**, 48 (4), 1323−1339.

(3) Gu, X.; Li, Y.; Hu, J.; Shi, Z.; Liang, F.; Huang, M. Elastic shear stiffness anisotropy and fabric anisotropy of natural clays. *Acta Geotech.* **2022**, 17, 3229−3243.

(4) Veytskin, Y. B.; Tammina, V. K.; Bobko, C. P.; Hartley, P. G.; Clennell, M. B.; Dewhurst, D. N.; Dagastine, R. R. Micromechanical characterization of shales through nanoindentation and energy dispersive x-ray spectrometry. *Geomech. Energy Envir.* **2017**, 9, 21−35.

(5) Fan, M.; Han, Y.; Tan, X.; Fan, L.; Gilliland, E. S.; Ripepi, N.; Chen, C. Experimental and numerical characterization of lower Huron Shale as a heterogeneous material. *Rock Mech. Rock Eng.* **2021**, 54 (8), 4183−4200.

(6) Huang, L.; Liu, J.; Zhang, F.; Donstov, E.; Damjanac, B. Exploring the influence of rock inherent heterogeneity and grain size on hydraulic fracturing using discrete element modeling. *Int. J. Solids Struct.* **2019**, 176−177, 207−220.

(7) Goral, J.; Deo, M.; McLennan, J.; Huang, H.; Mattson, E. Macro- and micro-compression testing of shales. *J. Petrol. Sci. Eng.* **2020**, 191, No. 107034.

(8) Dou, F. K.; Wang, J. G. A numerical investigation for the impacts of shale matrix heterogeneity on hydraulic fracturing with a two-dimensional particle assemblage simulation model. *J. Nat. Gas Sci. Eng.* **2022**, 104, No. 104678.

(9) Wang, Q.; Wang, T.; Liu, W.; Zhang, J.; Feng, Q.; Lu, H.; Peng, P. Relationships among composition, porosity and permeability of Longmaxi Shale reservoir in the Weiyuan Block, Sichuan Basin. *China. Mar Petrol Geol.* **2019**, 102, 33−47.

(10) Jarvie, D. M.; Hill, R. J.; Ruble, T. E.; Pollastro, R. M. Unconventional shale-gas systems: The Mississippian Barnett Shale of north-central Texas as one model for thermogenic shale-gas assessment. *AAPG Bull.* **2007**, 91 (4), 475−499.

(11) Rickman, R.; Mullen, M.; Petre, E.; Grieser, B.; Kundert, D. A practical use of shale petrophysics for stimulation design optimization: All shale plays are not clones of the Barnett Shale. In *SPE Annual Technical Conference and Exhibition. Society of Petroleum Engineers (SPE-115258)*; 2008.

(12) Sone, H.; Zoback, M. D. Mechanical properties of shale-gas reservoir rocks-Part 1: Static and dynamic elastic properties and anisotropy. *Geophysics.* **2013**, 78 (5), D381−D392.

(13) Sone, H.; Zoback, M. D. Mechanical properties of shale-gas reservoir rocks-Part 2: Ductile creep, brittle strength, and their relation to the elastic modulus. *Geophysics.* **2013**, 78 (5), D393−D402.

(14) Alsuwaidi, E. S.; Xi, G.; Zimmerman, R. W. Mechanical characterization of Laffan and Nahr Umr anisotropic shales. *J. Petrol. Sci. Eng.* **2021**, 200, No. 108195.

(15) Dou, F. K.; Wang, J. G.; Leung, C. F. The impacts of bedding strength parameters on the micro-cracking morphology in laminated shale under uniaxial compression. *Appl. Sci.* **2020**, 10 (16), No. 5496.

(16) Kaiser, P. K.; Kim, B. H. Rock mechanics advances for underground construction in civil engineering and mining. *Korea Rock Mech.* **2008**, 3−16.

(17) Amann, F.; Button, E. A.; Evans, K. F.; Gischig, V. S.; Blümel, M. Experimental study of the brittle behaviour of clay shale in rapid unconfined compression. *Rock Mech. Rock Eng.* **2011**, 44, 415−430.

(18) Amann, F.; Kaiser, P.; Button, E. A. Experimental study of brittle behaviour of clay shale in rapid triaxial compression. *Rock Mech. Rock Eng.* **2012**, 45, 21−33.

(19) Chen, B.; Zhang, Z.; Lan, Q.; Liu, Z.; Tan, Y. Experiment study on damage properties and acoustic emission characteristics of layered shale under uniaxial compression. *Materials.* **2023**, 16 (12), 4317.

(20) Duan, X.; Wang, W.; Liu, S.; Cao, Y.; Zheng, Z.; Zhu, Q. Experimental investigation on mechanical behaviour, energy evolution and gas permeability of anisotropic phyllite subjected to triaxial compression and cyclic loading. *Geomech. Energy Envir.* **2023**, 35, No. 100483.

(21) Liu, C.; Song, Z.; Zhang, D.; Zhao, H. Mechanical response of permeability evolution to anisotropic structure of reservoir rock under true triaxial stress path. *Geomech. Geophys. Geo-Energy Geo-Resour.* **2021**, 7 (3), 59.

(22) Agheshlui, H. Stress influence on the permeability of a sample heterogeneous rock. *Geomech. Geophys. Geo.* **2019**, 5 (2), 159−170.

(23) Hou, P.; Gao, F.; Yang, Y. G.; Zhang, X. X.; Zhang, Z. Z. Effect of the layer orientation on mechanics and energy evolution characteristics of shales under uniaxial loading. *Int. J. Min. Sci. Techno.* **2016**, 26 (5), 857−862.

(24) Dou, F. K.; Wang, J. G.; Zhang, X. X.; Wang, H. M. Effect of joint parameters on fracturing behaviour of shale in notched three-point-bending test based on discrete element model. *Eng. Fract. Mech.* **2019**, 205, 40−56.

(25) Shi, X.; Jiang, S.; Lu, S. F.; He, Z. L.; Li, D. J.; Wang, Z. X.; Xiao, D. S. Identification of mechanical properties of Longmaxi shale with beddings by nanoindentation tests: A case study on Silurian Longmaxi Formation of Youyang area in southeast Chongqing, China. *Petrol. Explor. Dev.* **2019**, *46* (1), 163−172.

(26) Gao, S.; Dong, D.; Tao, K.; Guo, W.; Li, X.; Zhang, S. Experiences and lessons learned from China's shale gas development: 2005−2019. *J. Nat. Gas. Sci. Eng.* **2021**, *85*, No. 103648.

(27) Guo, J.; Jia, C.; He, D.; Meng, F. Classification and evaluation on shale gas reservoir for Wufeng-Longmaxi Formation in Chuannan Area, Sichuan Basin. *Lithosphere* **2021**, *2021* (1), No. 3364731.

(28) Heng, S.; Guo, Y. T.; Yang, C. H.; Daemen, J. J. K.; Li, Z. Experimental and theoretical study of the anisotropic properties of shale. *Int. J. Rock Mech Min Sci.* **2015**, *74*, 58−68.

(29) Suo, Y.; Chen, Z. X.; Rahman, S. S.; Chen, X. Experimental study on mechanical and anisotropic properties of shale and estimation of uniaxial compressive strength. *Energ Source Part A* **2020**, 1−11.

(30) Zhang, K. Study on the effect of anisotropy of shale on mechanical properties and strain rate effect. Master degree thesis. Southwest University of Science and Technology, 2017.

(31) Hou, Z. K. Research on hydraulic fracturing tests and mechanism of crack extension of Longmaxi shale. Doctoral dissertation. Chongqing University, 2018.

(32) Rezaei, M.; Davoodi, P. K.; Najmoddini, I. Studying the correlation of rock properties with P-wave velocity index in dry and saturated conditions. *J. Appl. Geophys.* **2019**, *169*, 49−57.

(33) Zuo, J. P.; Wei, X.; Shi, Y.; Liu, C.; Li, M.; Wong, R. H. C. Experimental study of the ultrasonic and mechanical properties of a naturally fractured limestone. *Int. J. Rock Mech Min.* **2020**, *125*, No. 104162.

(34) Zhou, M. Y.; Zhang, Y. F.; Zhou, R. Q.; Hao, J.; Yang, J. J. Mechanical property measurements and fracture propagation analysis of Longmaxi shale by micro-CT uniaxial compression. *Energies* **2018**, *11* (6), 1409.

(35) Iyare, U. C.; Blake, O. O.; Ramsook, R.; Faulkner, D. R. Experimental study of the anisotropic behaviour of the Naparima Hill argillite. *Int. J. Rock Mech. Min. Sci.* **2022**, *153*, No. 105083.